Linearly polarised photon beams at ELSA

and measurement of the beam asymmetry in π^0-photoproduction off the proton

D. Elsner[1], B. Bantes[1], O. Bartholomy[2], D.E. Bayadilov[2,3], R. Beck[2], Y.A. Beloglazov[3], R. Castelijns[5,a], V. Crede[2,6], A. Ehmanns[2], K. Essig[2], R. Ewald[1], I. Fabry[2], K. Fornet-Ponse[1], M. Fuchs[2], C. Funke[2], A.B. Gridnev[3], E. Gutz[2], S. Höffgen[1], P. Hoffmeister[2], I. Horn[2], I. Jaegle[8], J. Junkersfeld[2], H. Kalinowsky[2], Frank Klein[1], Friedrich Klein[1], E. Klempt[2], M. Konrad[1], M. Kotulla[8,9], B. Krusche[8], H. Löhner[5], I.V. Lopatin[3], J. Lotz[2], S. Lugert[9], D. Menze[1], T. Mertens[8], J.G. Messchendorp[5], V. Metag[9], C. Morales[1], M. Nanova[9], D.V. Novinski[2,3], R. Novotny[9], M. Ostrick[1,b], L.M. Pant[9,c], H. van Pee[2], M. Pfeiffer[9], A.V. Sarantsev[2,3], C. Schmidt[2], H. Schmieden[1], B. Schoch[1], S. Shende[5], A. Süle[1], V.V. Sumachev[3], T. Szczepanek[2], U. Thoma[2], D. Trnka[9], D. Walther[1], C. Weinheimer[2,d], and C. Wendel[2]

(The CBELSA/TAPS collaboration)

1 Physikalisches Institut der Universität Bonn, Germany
2 Helmholtz-Institut für Strahlen- und Kernphysik der Universität Bonn, Germany
3 Petersburg Nuclear Physics Institute, Gatchina, Russia
4 Physikalisches Institut, Universität Erlangen, Germany
5 KVI, University of Groningen, The Netherlands
6 Department of Physics, Florida State University, Tallahassee, USA
7 Physikalisches Institut, Universität Basel, Switzerland
8 II. Physikalisches Institut, Universität Giessen, Germany

Abstract. At the electron accelerator ELSA a linearly polarised tagged photon beam is produced by coherent bremsstrahlung off a diamond crystal. Orientation and energy range of the linear polarisation can be deliberately chosen by accurate positioning of the crystal with a goniometer. The degree of polarisation is determined by the form of the scattered electron spectrum. Good agreement between experiment and expectations on basis of the experimental conditions is obtained. Polarisation degrees of $P_\gamma = 40\%$ are typically achieved at half of the primary electron energy. The determination of P_γ is confirmed by measuring the beam asymmetry, Σ, in π^0 photoproduction and a comparison of the results to independent measurements using laser backscattering.

PACS. 13.60.-r Photon and charged-lepton interactions with hadrons – 13.60.Le Meson production – 13.88.+e Polarization in interactions and scattering

1 Introduction

Experiments based on photo-induced exclusive reactions are well suited to improve our understanding of the complicated structure of the nucleon. In addition to measurements of cross sections, polarisation observables are indispensable. They are sensitive to interference terms and therefore give access to small amplitudes, even if those are too small to affect the total cross section significantly. Circularly and linearly polarised photon beams allow, in com-

a present address: FZ Jülich, Germany
b present address: University of Mainz, Germany
c on leave from Nucl. Phys. Division, BARC, Mumbai, India
d present address: University of Münster, Germany
Correspondence to: D. Elsner, Nussallee 12, 53115 Bonn, Germany, e-mail: elsner@physik.uni-bonn.de

bination with target or recoil polarisation, the extraction of double polarisation observables. From linearly polarised photons alone the beam asymmetry, Σ, can be extracted (for a definition of the observables see *e.g.* ref. [1]). In case of pseudoscalar meson photoproduction the beam asymmetry alone does not allow an unambiguous extraction of all partial waves [2], but its measurement is essential in view of a complete experiment [3].

The two common methods for generation of linearly polarised photons are coherent bremsstrahlung and Compton backscattering (CBS). In Compton backscattering the electron beam collides with a laser beam of short wavelength. Linearly polarised photons can be produced using linearly polarised laser photons [4,5]. The degree of polarisation of the CBS photons is proportional to that of laser photons, with its maximum at the highest photon energy.

At the present facilities this method is compared to electron bremsstrahlung limited in intensity and achievable maximum photon energy.

In coherent electron bremsstrahlung the recoil is transferred to a crystal radiator. Depending on its orientation relative to the electron beam, the whole crystal absorbs the recoil, which fixes the plane of electron deflection. Consequently, the photons produced by the coherent process are linearly polarised. Compared to CBS, photon beams from coherent bremsstrahlung have a higher intensity, but on the other hand a lower maximum degree of polarisation at higher photon energies.

Several facilities successfully use coherent bremsstrahlung to produce linearly polarised photons at high energies [6, 7]. For the first time a setup for coherent bremsstrahlung was installed and operated at the electron accelerator ELSA [8]. The following section is first devoted to the basics of coherent bremsstrahlung. The description of the apparatus is then followed by the alignment procedure for the crystal and the results obtained for the photon polarisation. In sect. 6 the measurement of the photon beam-asymmetry, Σ, in π^0-photoproduction is presented as an independent cross check for the polarisation analysis.

2 Coherent Bremsstrahlung

Radiators with a periodical lattice structure allow the production of linearly polarised photons via the process of coherent bremsstrahlung. In this section properties of the coherent process are described which are essential for the understanding of the experimental methods. For a more detailed discussion we refer to review articles [9–14].

In the case of incoherent bremsstrahlung (bs), an electron with energy E_0 and momentum $\boldsymbol{p_0}$ radiates a photon with energy k, due to coulomb interaction. Momentum conservation requires a recoil partner to take over the recoil momentum

$$\boldsymbol{q} = \boldsymbol{p_0} - \boldsymbol{p} - \boldsymbol{k}. \tag{1}$$

Here $\boldsymbol{p}$ denotes the momentum of the outgoing electron. In general, a kinematical constraint applies for the longitudinal, q_l, and transversal, q_t, momentum transfer. A good approximation for this so-called "pancake" condition [13, 14] is given by the relations
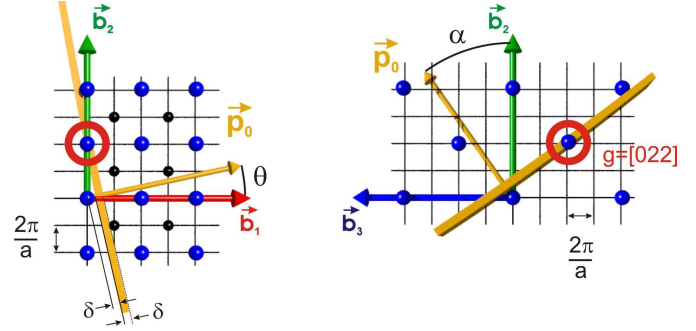
$$\delta \leq q_l \leq 2\delta \tag{2}$$
$$0 \leq q_t \leq 2x. \tag{3}$$

The longitudinal momentum transfer shows a non-zero lower limit given by

$$\delta(x) \equiv: q_l^{min} = \frac{1}{2E_0}\frac{x}{1-x}, \tag{4}$$

with the fractional photon energy x = k/E_0.

In the case of incoherent bs only one single nucleus (or electron) absorbs the momentum transfer, in contrast to the coherent process where the whole lattice participates, comparable to the Mößbauer effect. The process of

Fig. 1. Left: Projection of four parallel planes through the reciprocal lattice vectors [000], [001], [002] and [003] in the plane $\boldsymbol{b_1}$, $\boldsymbol{b_2}$. The primary momentum $\boldsymbol{p_0}$ is rotated by a small angle θ. The pancake region is indicated by a grey band. With regard to the $\boldsymbol{b_3}$-axis, perpendicular to the drawing plane, many vectors still lie in the allowed kinematical region (circle). Right: Reciprocal lattice vectors in the plane $\boldsymbol{b_2}$, $\boldsymbol{b_3}$. Compared to the left picture the angle θ is larger and $\boldsymbol{p_0}$ is tilted out of the plane $\boldsymbol{b_1}$, $\boldsymbol{b_2}$ by the angle α, such that only the vector [02$\bar{2}$] lies in kinematical allowed region.

coherent bs depends decisively on the orientation of the momentum transfer $\boldsymbol{q}$ in the reciprocal lattice space, more precisely, the momentum transfer has to fit to a vector of the reciprocal lattice. Consequently, only discrete recoil momenta can be transferred to the crystal as a whole, specified by the Laue condition

$$\boldsymbol{q} = n \cdot \boldsymbol{g}. \tag{5}$$

The reciprocal lattice vector

$$\boldsymbol{g} = \sum_{k=1}^{3} h_k \boldsymbol{b_k} \tag{6}$$

is composed of the Miller indices, h_k, and the basis vectors of the reciprocal lattice, b_k (below we use the nomenclature [$h_1h_2h_3$]). Figure 1 shows the momentum vector $\boldsymbol{p_0}$ in the reciprocal lattice space. For the selection of only one reciprocal lattice vector in the kinematical region of allowed recoils the angles θ in the plane $\boldsymbol{b_1b_2}$ and α in the plane $\boldsymbol{b_2b_3}$ have to be carefully chosen. The pancake region is illustrated by the grey band perpendicular to the momentum vector $\boldsymbol{p_0}$.

Contributions to the coherent bs cross section only result from reciprocal lattice vectors within the pancake region. At a fixed orientation of the lattice, the pancake shifts with increasing photon energy, cf. eq. 4. Consequently, at a certain point a reciprocal lattice vector leaves the pancake. This leads to a discontinuity in the coherent bs intensity at the fractional photon energy

$$x_d = \frac{2E_0\delta}{(1+2E_0\delta)}. \tag{7}$$

The plane of the electron deflection is fixed very tightly by the incoming electron momentum $\boldsymbol{p_0}$ and the reciprocal lattice vector $\boldsymbol{g}$ responsible for the coherent process. Hence, the linear polarisation of the emitted photons is oriented in the plane $(\boldsymbol{g}, \boldsymbol{p_0})$.
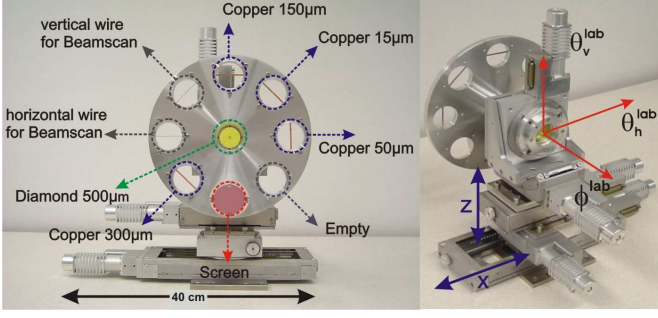
Fig. 2. Goniometer setup for the Crystal-Barrel/TAPS experiment at ELSA. Left: Available amorphous radiators which can be selected by rotation of the azimuthal axis. The horizontal translation allows the choice of either crystal or amorphous radiator. Right: Three step-motor drives may be used to rotate the crystal around a vertical axis (θ_v^{lab}), a horizontal axis (θ_h^{lab}) and an azimuthal axis (ϕ^{lab}). The diamond crystal is mounted in the center of the three axes with its [100] crystal axis parallel to the goniometer axis (ϕ^{lab}). The remaining two axes allow the horizontal and vertical translation.

3 Apparatus

The electron beam of ELSA [8] hits the radiator target in front of the tagging system [15]. Electron beams of $E_0 = 2.4\,\text{GeV}$ and $E_0 = 3.2\,\text{GeV}$ were routinely used for experiments with linearly polarised photons.

The crystal has a front surface of (4 x 4) mm and thickness of $500\,\mu\text{m}$. It is accurately positioned by a dedicated commercial 5-axis goniometer[1]. The maximum angular uncertainty is $\delta < 170\,\mu\text{rad}$ due to the wobble along the axes. Optical test measurements showed that other uncertainties, like absolute accuracy, uni-directional repeatability and reversal value (hysteresis) are negligible. The crystal, glued on a $12.5\,\mu\text{m}$ kapton foil, is positioned in the common center of the three rotation axes of the goniometer, horizontal (θ_h^{lab}), vertical (θ_v^{lab}) and azimuthal (ϕ^{lab}), cf. fig. 2. The minimum incremental motion (the smallest increment of motion the device is capable of consistently and reliably delivering) of each rotation axes is $\theta = 0.001\,\text{degree}$. Special measurements, discussed in sect. 4, confirm the orientation of the [100] crystal axis perpendicular to its front surface.

Further copper radiators with different thicknesses and wires to scan size and position of the electron beam are mounted on a disk around the crystal, as can be seen in fig. 2.

Electrons which radiated a photon are momentum analysed using the tagging-spectrometer, as schematically depicted in fig. 3. The detection system consists of 14 plastic scintillators providing fast timing and additional hodoscopes, a 480 channel scintillating fibre detector and a MWPC, to achieve a good energy resolution. The optimisation and analysis of linear polarisation is solely based on the data of the scintillating fibre detector which covers the energy range $E_\gamma = 0.18...0.8\,E_0$. The fibres are arranged

in two layers. The individual fibres overlap by around $2/3$ of their diameter. The energy resolution varies between $2\,\text{MeV}$ for the high photon energies and $25\,\text{MeV}$ for the low energies for $E_0 = 3.2\,\text{GeV}$. The tagged photon beam remains virtually uncollimated. Hence, the measured electron spectrum directly reflects the photon spectrum. The orientation of the linear polarisation and the position of the coherent maximum in the photon energy-spectrum depends on the alignment of the crystal relative to the electron beam direction. Maximum polarisation is found in the plane $(\boldsymbol{g}, \boldsymbol{p_0})$. The direction of the momentum vector $\boldsymbol{p_0}$ in the reference frame of the crystal is defined by the polar angle, θ, and the azimuthal angle, α, cf. fig. 1. The angle ϕ is the azimuth of the reciprocal lattice vector $\boldsymbol{g}$ in the same reference frame. Given θ and α, the position of the discontinuity, x_d, in the energy-spectrum can be calculated [14,6]:

$$x_d = [2E_0(g_1\cos\theta + \sin\theta(g_2\cos\alpha + g_3\sin\alpha))] \qquad (8)$$
$$\cdot[1 + 2E_0(g_1\cos\theta + \sin\theta(g_2\cos\alpha + g_3\sin\alpha))]^{-1}.$$

Relations between crystal angles (θ, α, ϕ) and goniometer angles $(\theta_h^{lab}, \theta_v^{lab}, \phi^{lab})$ for the g=$[02\bar{2}]$ reciprocal lattice vector are given by [6]

$$\theta_v^{lab} = \arcsin(\sin\theta\,\sin(\alpha + \phi^{lab})); \qquad (9)$$
$$\theta_h^{lab} = -\arctan(\tan\theta\,\cos(\alpha + \phi^{lab})); \qquad (10)$$
$$\theta = \arccos(\cos\theta_h^{lab}\,\cos\theta_v^{lab}); \qquad (11)$$
$$\alpha = \arccos[(-\cos\phi^{lab}\sin\theta_h^{lab}\cos\theta_v^{lab}$$
$$+ \sin\phi^{lab}\sin\theta_v^{lab})(\sin\theta)^{-1}]; \qquad (12)$$
$$\phi = \phi^{lab} + \beta. \qquad (13)$$

The angle β defines the orientation of the polarisation plane, $\beta = 0$ and $\pi/2$ are associated to vertical and horizontal linear polarisation, respectively. It is essential to determine all angular offsets between the crystal reference frame and the goniometer system on the one hand, and the incoming electron beam and the goniometer system on the other hand with sufficient accuracy. The former offsets have to be measured once in case of a fixed installation. The latter depend on the stability of the beam alignment and have to be determined repeatedly. For the alignment process we use the coherent bremsstrahlung itself as described in the next section.
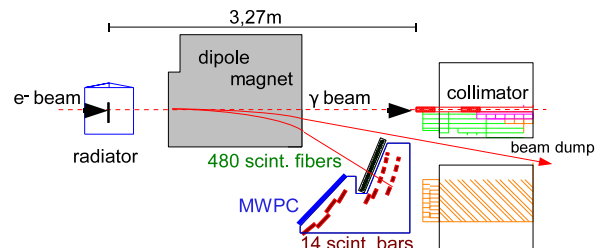
Fig. 3. Setup of the tagging-system as described in the text.
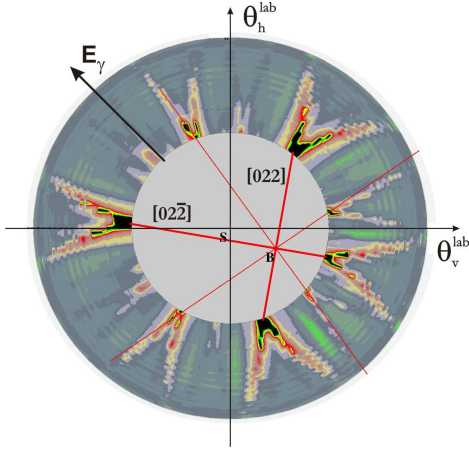
Fig. 4. Stonehenge plot for non aligned crystal at an electron-beam energy of E_0=3.2 GeV. The tagged photon energy is plotted radially, the colour-code (greyscales) represents the coherent intensity. The axes show the horizontal and vertical rotation in the goniometer system. The opening cone of the quasi azimuthal scan is $\theta_c = 60$ mrad, see eq. 15. The prominent structures associated to the [022] and [02$\overline{2}$] reciprocal lattice vectors. The structures rotated by 45 degrees result from the [044] and [04$\overline{4}$] vectors and give additional interpolation points .

4 Crystal alignment - Stonehenge Technique

The alignment is achieved by the *Stonehenge Technique*. The procedure can cope with a relatively large mounting misalignment and allows any arbitrary orientation of the polarisation plane to be selected. A detailed description is given in [16,17]. The basis of the technique is a quasi azimuthal scan which sweeps the crystal axes in a cone of angular radius θ_c by stepping simultaneously on the horizontal and vertical axis of rotation:

$$\theta_v^{lab} = \theta_c \cos\Phi; \quad 0 \le \Phi < 2\pi \qquad (14)$$

$$\theta_h^{lab} = \theta_c \sin\Phi. \qquad (15)$$

For each point of the scan a photon energy spectrum is measured and plotted in a polar diagram (*Stonehenge plot*), where the photon energy increases in the outward radial direction and the x- and y-directions correspond to the rotation axes θ_v^{lab} and θ_h^{lab}, respectively. In order to accentuate the coherence effect, the spectra are normalised to the spectrum of an amorphous copper radiator. Therefore the colour code of the diagram denotes the coherent intensity. A Stonehenge plot for a non aligned crystal taken for the Crystal-Barrel/TAPS experiment [2] is shown in fig. 4. The coherent contributions from different settings of crystal planes result in pronounced structures due to the different angles between crystal and electron beam. The strongest intensities typically relate to the [022] and [02$\overline{2}$] reciprocal lattice vectors and the points where they converge at $E_\gamma \to 0$ (inner circle) indicate where the corresponding setting of planes is parallel to the electron
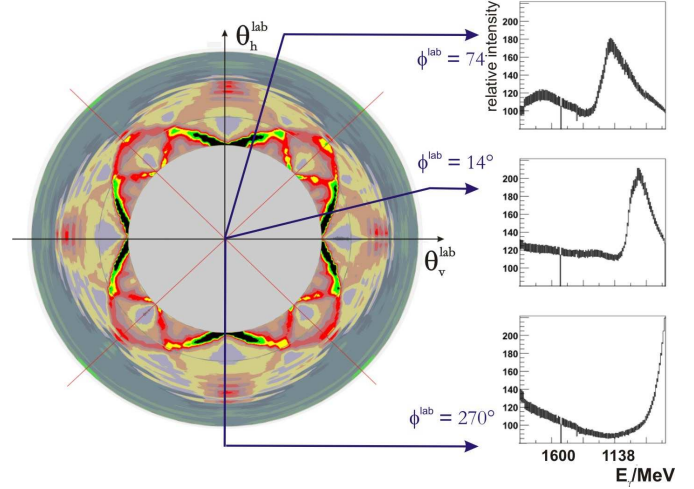
Fig. 5. Stonehenge plot for perfect aligned crystal at E_0=3.2 GeV, cf. fig. 4. Here the opening cone of the quasi azimuthal scan is $\theta_c = 10$ mrad. Photon energy spectra for three different ϕ-angles are plotted additionally to illustrate the shifting of the coherent peak.

beam. The analysis of the symmetry in the Stonehenge plots yields all independent offsets of the crystal. For a detailed description of this analysis method it is referred to [16,17].

Taking into account the angular offsets, it is possible to set the linear polarisation at any desired spatial direction and at any photon energy by choosing the crystal orientation. Figure 5 shows the Stonehenge plot of a perfectly aligned crystal with a vertical orientation of the [022] plane. Three one-dimensional sample histograms for different directions are shown on the right side. The precision of the angular offsets depends on scan parameters, basically the step size and the cone θ_c (cf. eq. 15). The resulting azimuthal orientation has an accuracy of $\Delta\phi = 0.5$ degree [17].

In order to preserve the alignment during the experiment, the stability of the beam position is monitored online, using the coherent peak itself, since the position of the coherent peak in the energy spectrum is extremely sensitive to angle of the incident beam. As for the Stonehenge plots, also for beam diagnostics the coherent spectrum is always normalised to the spectrum of an amorphous copper radiator. At the beginning of each experiment a normalised reference histogram is defined, which is compared with the online spectrum permanently. The incoherent copper spectrum is measured in regular intervals.

5 Degree of linear polarisation

The generation of high degrees of linear polarisation requires the isolated contribution of one of the [0,±2,±2,] reciprocal lattice vectors to coherent bremsstrahlung. Precisely determined offsets (cf. sect. 4) enable to deliberately set both, the energy of the coherent peak and the orientation of the linear polarisation. The determination
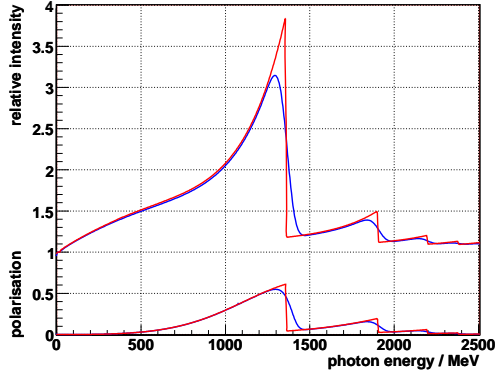
Fig. 6. Comparison of the polarisation contribution of the [04$\overline{4}$] vector, with its maximum at E_γ=1900MeV, underneath the selected [02$\overline{2}$] vector at E_γ=1300MeV. The curve with the broadened peaks shows the effect of typical experimental conditions, basically multiple scattering and electron-beam divergence.

electron energy	3176.1 MeV
spot size $\sigma_{horizontal}$	1.5 mm
spot size $\sigma_{vertical}$	1.0 mm
divergence $\sigma^p_{horizontal}$	0.3 mrad
divergence $\sigma^p_{vertical}$	0.08 mrad

Table 1. Electron beam properties.

crystal thickness	0.5 mm
calculated numbers of lattice vectors	1000
incoherent scaling factor	1.35

Table 2. Radiator properties.

$E_\gamma(P^{max.})$/MeV	$P^{max.}$	θ_h^{cry}/mrad	θ_v^{cry}/mrad
1305	0.49	-3.16	-56.78
1515	0.42	-4.09	-64.00
1610	0.39	-4.58	67.00
1814	0.31	-5.88	76.00

Table 3. Coherent peak position, maximum degree of polarisation, $P^{max.}$, and crystal angles for the vertical orientation of the polarisation plane.

of the polarisation degree is based on the comparison of the measured electron spectrum with the ANB ("analytic bremsstrahlung calculation") software [19] from Tübingen University. The ANB code allows the calculation of coherent intensities for each single reciprocal lattice vector. It integrates over all desired vectors. Taking into account the incoherent contributions, the degree of polarisation can be determined. If there is no overlap of different reciprocal lattice vectors within a given energy interval, the degree of polarisation can be obtained from *any* fit of the intensity spectrum.

Figure 6 shows the ANB-calculated relative photon intensity spectrum along with the calculated photon polarisation. Due to a tiny overlap with the adjacent peak of the [04$\overline{4}$] vector the exact determination of the polarisation degree from the experimental data alone is not feasible. In our particular case no clear separation of the vector [02$\overline{2}$] was realisable in the required energy region.

Under given experimental conditions the shape of the coherent spectrum is not determined by the crystal orientation alone. Each single process has a small deviation from the nominal kinematics as a result of beam divergence and multiple scattering in the crystal. Both effects cause a smearing of the sharp edge at the discontinuity position, due to the different pancake conditions for individual processes, and hence lower the intensity and consequently the maximum degree of polarisation (cf. fig. 6). The effects of beam divergence, beam spot-size, energy resolution and multiple scattering are included in the ANB software. Tables 1-3 show overviews of typical values for our experimental parameters. The electron-beam energy and the spot size are precisely measured. The values of the beam divergence result from calculations of the beamline optic.

Additionally, collimation affects the degree of polarisation, due to the different angular distribution for the coherent and incoherent bs. However, no effective collimation of the photon beam was used in the experimental.

During the first round of CBELSA/TAPS data taking at ELSA four different crystal settings were used, with maximum polarisation at E_γ=1305 MeV, 1515 MeV, 1610 MeV and 1814 MeV. Vertical orientation of the polarisation vector was chosen, since the vertical divergence of the ELSA electron beam is about an order of magnitude smaller than in horizontal direction. Normalised electron spectra are shown in fig. 7. The curves represent a calculation using an improved version [22] of the original ANB software. The description of the measured intensity spectrum is very accurate at all settings. Two main improvements in the ANB code were necessary to obtain this level of agreement between calculation and experimental data. The inclusion of multiple scattering was improved by a more precise approximation of the angular distribution [23]. The original description [24] only accounts for the first order of the series expansion of the scattering angle in Molière theory. This accuracy was not sufficient to describe the experimental spectrum. As a consequence a discrepancy appears in the steep edge of the coherent peak.

Furthermore, the *incoherent* description of the ANB software needs to be scaled for all calculations by a factor of 1.35 (cf. table 2). This was traced back to an uncertainty in the parametrisation of the atomic form factor. A scaling of the atomic form factor according to Cromer and Waber [18] by a factor of 1.1 yields the same result, as the scaling of the incoherent part. Taking into account the formfactor parametrisation after Schiff [20], the difference of the form factors is also a factor of 1.1. Consequently, the two alternative parametrisations provide an uncertainty in the order of 10% in the required momentum-transfer region. The relative strengths of coherent and incoherent
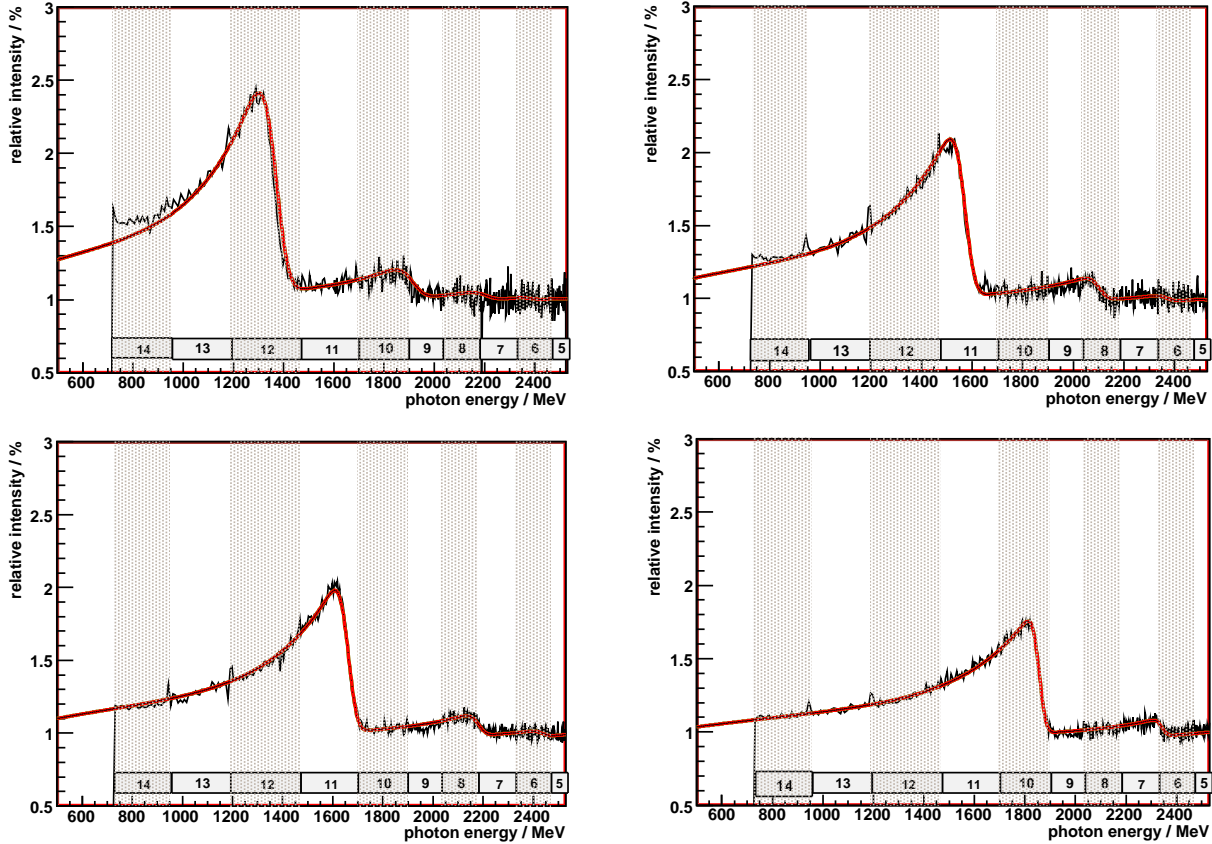
Fig. 7. The measured coherent bremsstrahlung intensity normalised to an incoherent spectrum in comparison to an improved version [22] of the ANB-calculation [19] (full curve). The diamond radiator was set for an intensity maximum at $E_\gamma = 1305\,\text{MeV}$ (top left), $E_\gamma = 1515\,\text{MeV}$ (top right), $E_\gamma = 1610\,\text{MeV}$ (bottom left), $E_\gamma = 1814\,\text{MeV}$ (bottom right). The numbered blocks indicate the ranges covered by the 14 timing scintillators of the tagging detector.

contributions determine the absolute value of linear polarisation. In this respect the re-scaling of the incoherent contributions introduces no significant additional error.

An absolute error of $\delta P_\gamma < 0.02$ is estimated using variations of the calculated relative intensity by $\pm 5\%$. These worst-case estimate accounts for deviations from the shape of the spectrum due to combined statistical and systematical effects.

Assigning the appropriate photon energy to each single event in the data analysis yields the event-weighted average polarisation in each bin of photon energy. An independent cross check of the determination of the polarisation degree is the measurement of the photon beam-asymmetry, Σ, in an energy region were it is well known from other independent measurements. This is discussed in the next section.

6 Beam asymmetry in π^0 photoproduction

The analysis of the photon beam-asymmetry, Σ, in the reaction $\gamma p \to p\pi^0$ provides a well suited consistency check for the determination of the degree of polarisation. Large

photon asymmetries are involved, especially at small angles $\theta_{\pi^0}^{cm}$, and a zero-crossing at certain energies. Comparing our results to earlier measurements at GRAAL[2] [5] gives an independent check, in particular because at GRAAL linearly polarised photon beams are produced by a different process, laser backscattering, with a well defined and high degree of polarisation. Our results are based on the same data set and data analysis presented in a previous publication on the beam asymmetry in η photoproduction [2]. The experimental setup and the main steps of the data analysis are shortly summarised in the following.

6.1 Experimental setup and data analysis

The linearly polarised photon beam from the tagging system (cf. Sec. 3) was incident on a 5.3 cm long liquid hydrogen target. The target is surrounded by a cylindrical, three layer scintillating fibre detector, covering the polar angular range from 15 to 168 degrees, and the `Crystal Barrel` (CB) detector [25], consisting of 1290 individual

---

[2] **GR**enoble **A**nneau **A**ccelerateur **L**aser
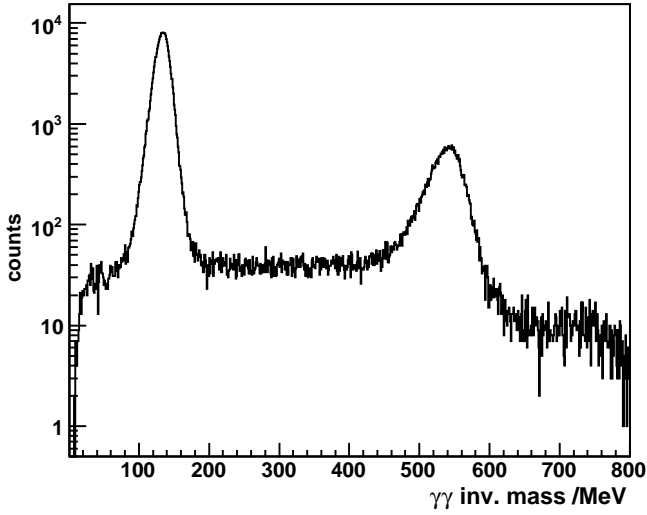
Fig. 8. Two photon invariant mass distribution from the full energy and angular range after the standard kinematic analysis cuts (see text). Signal widths of $\sigma_{\pi^0} = 10$ MeV and $\sigma_\eta = 22$ MeV are obtained. Note the logarithmic scale.

CsI(Tl) crystals covering a polar angular range of 30 — 168 degrees. The forward cone of 5.8 — 30 degree was covered by the `TAPS` detector, a setup of 528 BaF_2 modules at a distance of 118.7 cm from the target. Charged particle recognition is obtained by the hit information from the plastic-scintillator modules in front of `TAPS` and the scintillating fibre detector inside CB. The first level trigger was derived from the `TAPS` detector modules, which are individually equipped with photomultiplier readout. Two alternative trigger conditions were used, either ≥ 2 hits above a low threshold (A) or ≥ 1 hit above a high threshold (B). Within $\simeq 10\,\mu$s, a fast cluster recognition for the `Crystal Barrel` provides the second level trigger (C). Finally, the total trigger condition required 2 clusters identified: $[A \vee (B \wedge C)]$.

The offline analysis is based on three detector hits, corresponding to two photons from the pion decay, and the proton. A photon hit is usually composed of a cluster of adjacent crystals whose energy is summed over. Due to the detection of the proton, the kinematics is overdetermined. The analysis starts with all combinatorial possibilities, *i.e.* 3 for the 3–cluster events. No charged particle identification for the proton was used to avoid false azimuthal distributions due to inefficiencies of the veto detectors. Furthermore, only the angular information of the proton candidate was used. The energy of the proton candidate was disregarded.

Kinematic cuts, based on longitudinal and transverse momentum conservation, are used to extract the desired reaction. Additionally, a cut on the missing mass was applied to the proton candidates ($m_p \pm 150$MeV). Figure 8 shows the two-photon invariant mass distribution [2] obtained. Below the π^0 and η peaks the overall background is very small (note the logarithmic scale). After background subtraction a clean event sample was obtained from cuts of

3σ width around the π^0 mass in the invariant mass spectra.

The cross section of pseudoscalar meson photoproduction off a nucleon with linearly polarised beam [27] is given by

$$\frac{d\sigma}{d\Omega} = \frac{d\sigma_0}{d\Omega} \left(1 - P_\gamma \, \Sigma \, \cos 2\Phi \right). \qquad (16)$$

the beam asymmetry, Σ, can be extracted from the modulation of the cross section over the azimuth. In eq. 16 σ_0 denotes the polarisation independent differential cross section, P_γ the degree of linear polarisation of the incident photon beam, and Φ the azimuthal orientation of the reaction plane with respect to the plane of linear polarisation. From a fit of the azimuthal event distribution

$$f(\Phi) = A + B \, \cos(2\Phi) \qquad (17)$$

the product of beam asymmetry and photon polarisation, $P_\gamma \Sigma$, is given by the ratio B/A in each bin of photon energy and pion angle, $\theta_{\pi^0}^{cm}$. Finally, the event-weighted average polarisation, assigned as described in Sec. 5, allows the determination of Σ in each data bin.

6.2 Results

Figure 9 shows the results for the beam asymmetry extracted for one crystal setting with a maximum degree of polarisation at $E_\gamma = 1305$ MeV. Statistical errors are directly attached to the data points. The bars indicate the estimated total systematic uncertainty. The major contribution to the systematic error of this experiment stems from angle-dependent inefficiencies [22]. Data within the range $\theta_{\pi^0}^{cm} = 60 - 100$ degree are missing due to the trigger condition B, which was used to select events with higher photon multiplicity than $\pi^0 \to 2\gamma$. In fig. 9 our data are compared to data of the GRAAL collaboration [5]. Both data sets show a very good agreement, despite small fluctuations around $\theta_{\pi^0}^{cm} = 115$ degree. The kinematics of these data points are correlated to a very low proton energy, probably the protons got stuck in the ϕ-unsymmetrical holding structure of the inner detector. This ϕ-dependence of detection efficiency affects directly the experimental asymmetry.

Figure 9 also shows the good agreement between both data sets and two standard calculations, the Mainz isobar model `MAID` [28] and the Bonn–Gatchina partial wave analysis `BnGa` [29].

An explicit deviation of both data sets is shown in fig. 10. The difference of the absolute values of the beam asymmetries ($|\Sigma_{CB}| - |\Sigma_{GRAAL}|$) is plotted in one histogram. This representation is more sensitive to an incorrect measurement of the photon polarisation than the difference of the signed values. In fig. 10 the mean value of a gauss distribution is compatible with zero. Also the width (sigma) corresponds to our mean statistical error. Consequently this cross check shows no indications for an additional contribution to the systematic error in the determination of the degree of polarisation. Hence we conclude that the absolute determination of the degree of linear polarisation
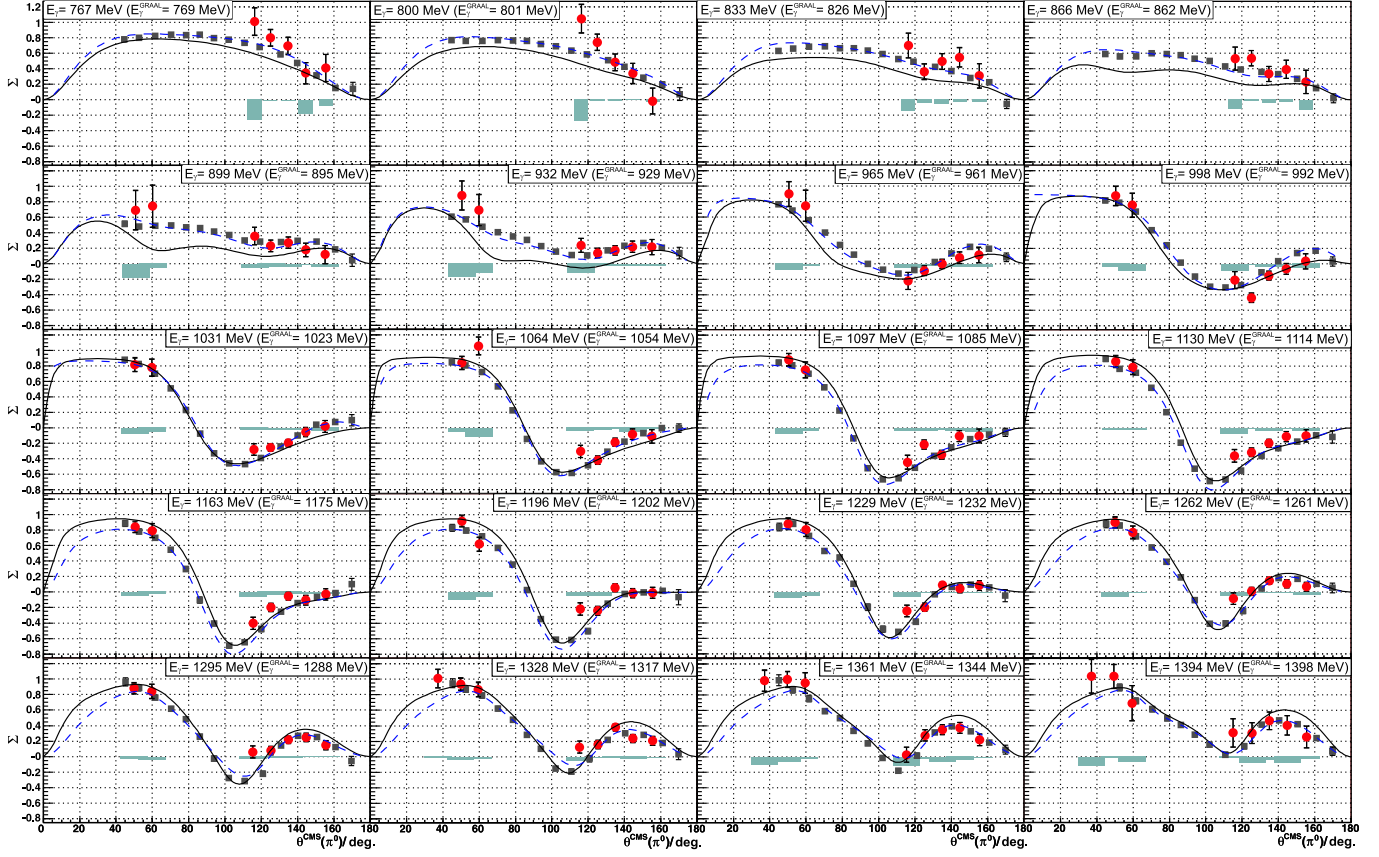
Fig. 9. The beam asymmetry Σ *versus* $\theta_{\pi^0}^{cm}$ for the reaction $\gamma p \to p\pi^0$. CBELSA/TAPS data (circles) with statistical errors. The systematic error [2] is indicated by the bar chart. Our data are compared to data of the GRAAL collaboration [5] (boxes). The curves represent calculations of `MAID` [28] (full) and Bonn–Gatchina partial wave analysis `BnGa` [29] (dashed). Data within the range $\theta_{\pi^0}^{cm} = 60 - 100$ degree are missing due to the trigger condition, see text.

is under control on the level of the estimated errors given in sect. 5.

7 Summary

We have presented the method to produce a linearly polarised photon beam at ELSA by means of coherent bremsstrahlung off a diamond crystal. Within the photon energy range $E_\gamma = 800...1400\,\text{MeV}$ we achieve polarisation degrees up to $49\,\%$. At higher energies the polarisation reduces to *e.g.* $P_\gamma \approx 30\%$ at $E_\gamma = 1800$ MeV. The precise orientation of the diamond crystal *versus* the incoming electron beam is essential. It is realised by a 5-axis goniometer. The alignment is based on the *Stonehenge Technique*. Both, the relative intensity spectrum and the polarisation degree, have been calculated with an improved version of the ANB software.

An independent consistency check is provided by the measurement of the photon beam asymmetry, Σ, in the reaction $\gamma p \to p\pi^0$. The combined setup of the `Crystal Barrel` and `TAPS` detectors enabled a high-resolution detection of multiple photons, important for the clean de-
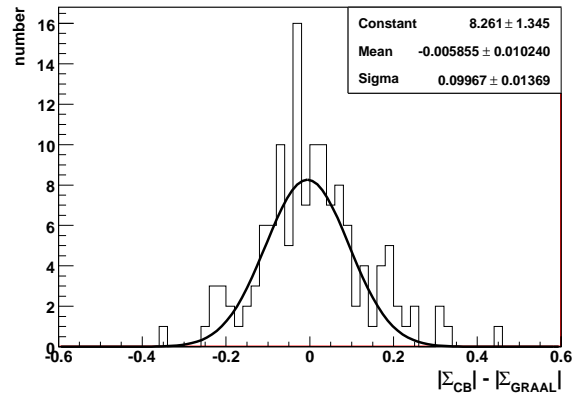
Fig. 10. The difference of the absolute values of the beam asymmetries from our experiment and the results from the GRAAL collaboration [5]. Each difference of two data points corresponds to one entry in the histogram. In order to ensure the same kinematics of both data sets the GRAAL data are linearly interpolated in E_γ and $\theta^{CMS}(\pi^0)$ to our mean values.

tection of the 2γ decays of the pion. The obtained photon asymmetries are compared with a previous measurement by the GRAAL collaboration. A very good overall consistency of the data sets is obtained. No deviations were visible beyond the error of $\delta P_\gamma < 0.02$ given above. The production of linearly polarised photons via coherent bremsstrahlung and the presented method of determination of the degree of polarisation is now routinely used as a standard technique at ELSA.

References

1. G. Knöchlein, D. Drechsel and L. Tiator, Z. Phys. **A352**, 327 (1995).
2. D. Elsner *et al.*, Eur. Phys. J. **A33**, 147 (2007).
3. W.-T. Chiang and F. Tabakin, Phys. Rev. **C55**, 2054 (1997).
4. T. Nakano *et al.*, Nucl. Phys. **A684**, 71c (2001).
5. O. Bartalini *et al.*, Eur. Phys. J. **A26**, 399 (2005).
6. D. Lohmann *et al.*, Nucl. Instr. and Meth. **A343**, 494 (1994).
7. P.L. Cole *et al.*, proceedings GDH 2002 Genova, World Scientific Publishing Co. Pte. Ltd.
8. W. Hillert, Eur. Phys. J. **A28**, 139 (2006).
9. F.H. Dyson and H. Überall, Phys. Rev. **99**, 604 (1955).
10. H. Überall, Phys. Rev. **103**, 1055 (1956).
11. H. Überall, Phys. Rev. **107**, 223 (1957).
12. H. Überall, Z. Naturforsch. **17a**, 332 (1962).
13. G. Diambrini Palazzi, Rev. Mod. Phys. **40**, 611 (1968).
14. U. Timm, Fortschritte der Physik **17**, 765 (1969).
15. K. Fornet-Ponse, Eur. Phys. J. **A**, *The photon tagging system of the CB-experiment at ELSA, in preparation* (2008).
16. K. Livingston, International Conference on Charged and Neutral Particles Channeling Phenomena, Proc. SPIE, (2005).
17. K. Livingston, Nucl. Instr. and Meth. *The Stonehenge Technique. A new method of aligning crystals for linearly polarized photon production from coherent bremsstrahlung, in preparation* (2008).
18. D.T. Cromer and J.T. Waber, Acta. Cryst. **18**, 104 (1965).
19. F.A. Natter *et al.*, Nucl. Instr. Meth. **B211**, 465 (2003).
20. L.I. Schiff, Phys. Rev. **83**, 252 (1951).
21. J.H. Hubbell, J. Appl. Phys. **30**, 981 (1959).
22. D. Elsner, doctoral thesis, Bonn (2006) `http://hss.ulb.uni-bonn.de/diss_online/math_nat_fak/2007/elsner_daniel/index.htm`.
23. G.R. Lynch and O.L. Dahl, Nucl. Instr. Meth. **B58**, 6 (1991).
24. A.O. Hanson *et al.*, Phys. Rev. **84**, 634 (1951).
25. E. Aker *et al.*, Nucl. Instr. Meth. **A321**, 69 (1992).
26. R. Novotny *et al.*, IEEE transaction on nuclear science **38**, 378 (1991).
27. D. Drechsel, S.S. Kamalov and L. Tiator, Nucl. Phys. **A645**, 145 (1999).
28. W.T. Chiang, S.N. Yang, L. Tiator, D. Drechsel, Nucl. Phys. A **A700**, 429 (2002).
29. A.V. Anisovich *et al.*, Eur. Phys. J. **A25**, 427 (2005).